International Refrigeration and Air Conditioning Conference

School of Mechanical Engineering

2021

Measurement Of Film Thickness And Temperature On Horizontal Metal Spray Coated Tube Falling Film Evaporator Using Interferometric Techique

Akhil Krishnan Maliackal
Indian Institute of Technology Madras, India

Ganesan A R

Mani Annamalai
Indian Institute of Technology Madras, India, mania@iitm.ac.in

Follow this and additional works at: https://docs.lib.purdue.edu/iracc

Maliackal, Akhil Krishnan; A R, Ganesan; and Annamalai, Mani, "Measurement Of Film Thickness And Temperature On Horizontal Metal Spray Coated Tube Falling Film Evaporator Using Interferometric Techique" (2021). *International Refrigeration and Air Conditioning Conference.* Paper 2139.
https://docs.lib.purdue.edu/iracc/2139

Measurement of film thickness and temperature on horizontal thermal spray coated tube falling film evaporator using interferometric technique

Akhil Krishnan Maliackal[1], A.R. Ganesan[2], A. Mani[3*]

[1] Department of Mechanical Engineering, Indian Institute of Technology Madras, India
me15d403@smail.iitm.ac.in

[2] Department of Physics, Indian Institute of Technology Madras, India
arg@iitm.ac.in

[3] Department of Mechanical Engineering, Indian Institute of Technology Madras, India
mania@iitm.ac.in

* Corresponding Author

ABSTRACT

'Water' is the 'Essence of Life'. It is an irreplaceable precious resource that is core of life on earth, a vital commodity that is critical for human survival, socio-economic developments and for the preservation of a healthy ecosystem. Current trends indicate that two-thirds of the world's population will be living in water-stressed countries by 2025(wat (2006)). In order to eradicate or to provide sufficient water requirement for mankind desalination plays a pivotal role.

This paper presents studies on horizontal tube falling film evaporator for Multi effect desalination (MED) system with spray coated tubes. The most important component in any MED system is the falling film evaporator. The wide acceptance for this kind of evaporators is because of the fact that it is characterized by a very low-pressure drop. In MED systems, falling film evaporation takes place outside the tube geometry utilizing the latent heat of condensing vapour inside the tube. Convective evaporation, as well as low-temperature nucleate boiling, occur in the film as it flows over the tube depending on the operating conditions(Abraham and Mani (2015)). The liquid falls on the top of the tube and flows down along the curved tube surface. There is a phase change on both sides of the tube and the evaporation outside the tube helps vapour to be separated from the liquid as soon as it is formed.

Two different tubes surfaces were studied, namely bare copper tube and copper tube coated with alloy of Al_2O_3 and TiO_2. Scanning electron microscope, Energy-dispersive X-ray spectroscopy, 3D surface profilometer were utilized to study about the surface texture, composition and to find surface roughness values attributed with each tubes.

An optical shadow method (non-intrusive) incorporating Otsus's algorithm was used to evaluate the film thickness around the circumference of the cylinder, and a Mach-Zehnder Interferometer (MZI) was employed to visualize the isotherm formation (Maliackal et al. (2021)). All studies were performed for complete wetting of the tube. The measured film thickness was compared with commonly used empirical formulas. Further, the effectiveness of using those empirical formulas for small diameter tubes was analyzed. A novel interferometric technique was used to analyze the film interface temperature, and a comparative study was performed for the two different tube geometries. A standard error of mean (SEM) analysis was performed on every data set.

1. INTRODUCTION

Falling film is a delicate thin fluid structure. In order to study the essential characteristics such as film thickness and interface temperature, non-intrusive type of measurements are the best choice as they carry out measurements in proximity without disturbing the structure. But the main challenge arising in most of

the non-intrusive falling film thickness measurements was its incapability to measure the entire perimeter of the cylinder because of the experimental constraints (Chen et al. (2015),Jayakumar et al. (2019),Gstoehl et al. (2010)). In this paper, we present an optical shadow method (non-intrusive) for evaluating the falling film thickness around the circumference of a horizontal tube evaporator in the range $5° \leq \theta \leq 175°$. The Otsu's algorithm was incorporated for analysising the images which is known to be the best when an abrupt change in pixel to pixel intensity frequencies occurs. At state of the art, the research works carried out to measure film interface temperature are scarce (Zhang et al. (2009),Borgetto et al. (2013)). In this study, a MZI is used to qualitatively and quantitatively analyse the isotherm formation associated with the horizontal tube falling film evaporator. A novel interferometric method is developed to accurately track the local falling film interface temperature. The studies were performed for two different tube surfaces, namely bare copper tube and $Al_2O_3 + TiO_2$ alloy coated tube and the comparisons are drawn, which will be discussed in detail later.

2. SYSTEM CHARACTERISTICS

A horizontal tube falling film evaporator was fabricated on an SS316 body. A water bath provided an uninterrupted supply of constant temperature feed inlet water. An optimally designed feed distributor along with three dummy tubes provide a thin uniform flow over the test tube, as shown in Fig. 1a. The test tube is maintained isothermally using a cylindrical cartridge heater and an associated PID controller setup as depicted in Fig. 1a. The test tube is fabricated in copper with an outer diameter of 15.9 mm. The impingement height was designed to be 9 mm. A photograph of the test setup is shown in Fig. 1b.

**(a)**   **(b)**
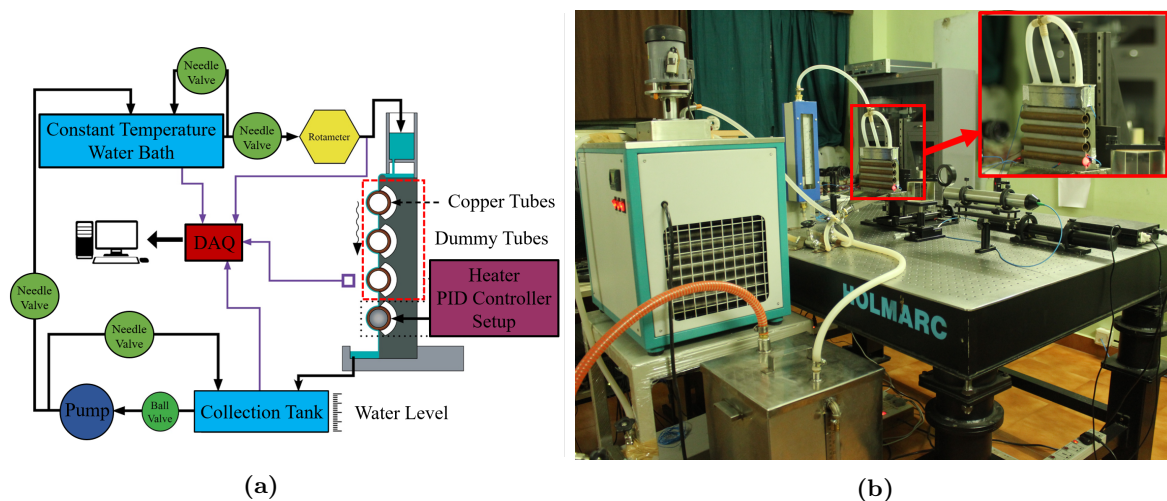
Figure 1: (a) Schematic of falling film evaporator experimental setup (b) Photograph of falling film evaporator experimental setup

Table 1: Operating Conditions and system characteristics

Operating Fluid	Distilled Water
Operating Flow Rate (LPM)	0.068 kg·m^{-1}·s^{-1}.
Operating Temperature (T-type)	80–110 with an accuracy of $\pm$ 0.1 ˚C for entire range
Mean F.I.T and B.T	90.1 ˚C and 105.3 ˚C
Thermal spray coating material	$Al_2O_3 + TiO_2$
Thermal spray coating thickness	100μm
Thermal spray coating R$_a$ value	6.11μm
Thermal spray coating porosity	2.2%
Bare copper tube R$_a$ value	1.3μm

Two different tubes were studied in this paper viz. bare copper tube and a thermal spray-coated tube with
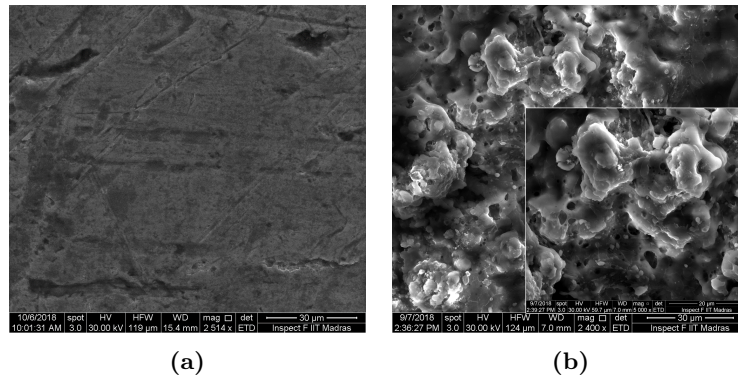
Figure 2: Scanning electron microscope image of (a) bare tube and (b) Al_2O_3 + TiO_2 spray coated tube.
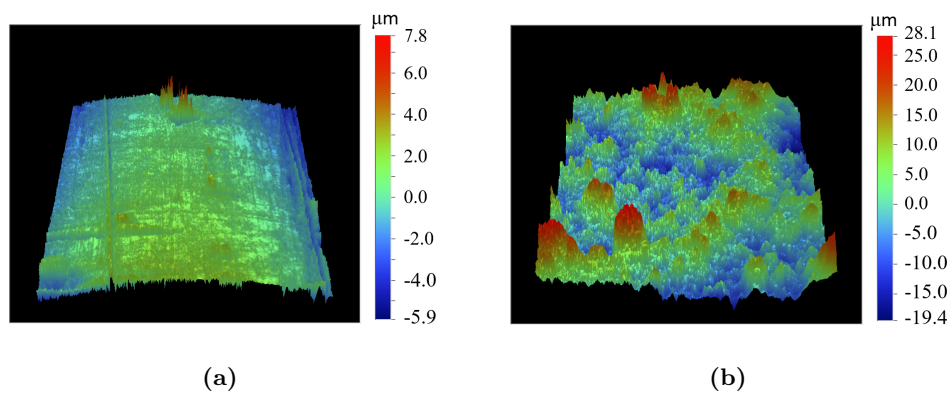
**Figure 3:** 3D surface profile of (a) bare tube and (b) Al_2O_3 + TiO_2 spray coated tube.

Al_2O_3 + TiO_2. The scanning electron microscope images are given in Fig. 4. The 3D surface profile study for the tubes were carried out to get insight into surface roughnesses and the profiles obtained are as shown in Fig. 3. The system and tube properties for the present study is illustrated in Table. 1.

The measurement of the contact angle provides qualitative information of the wettability of the surface. A material can be defined as a wetting surface, provided the contact angle is less than 90° and is directly correlated to the hydrophilicity or wettability (Law (2014)). Figures 4a and 4b show the snapshots for measured contact angles using an aqueous sessile drop placed on the two different surfaces. The average contact angles measured are 73.3^o and 49.95^o respectively for bare copper tube, and Al_2O_3 +TiO_2 thermally spray-coated tube. It is already known that the wettability will be modified by the surface roughness, which scales with the ratio of actual surface area to the smooth surface area having the same geometric shape and dimension (Wenzel (1949)). Hence the diminution in the contact angle measured for the thermally coated surface represents the wettability enhancement and spreading of fluid.

3. THEORY AND EXPERIMENT CONDUCTED

3.1 Falling film interface temperature measurement

Refractive index of a homogeneous medium is a function of the thermodynamic state, often only the density. The decrease in the speed of light while travesing through a test section of varying refractive index can be viewed as an increase in the optical path length which has to be traversed by the electromagnetic waves and will act as the source of phase difference. A MZI was used for capturing the path length difference as illustrated in Fig. 5. A laser source was used along with a collimating arrangement to achieve the required beam size . Beam Splitter 1 (BS1), Mirror 1 (M1), Mirror 2 (M2) and Beam Splitter 2 (BS2) are all placed 45˚ with respect to the laser beam direction. BS1 splits the incoming laser beam into transmitted beam and
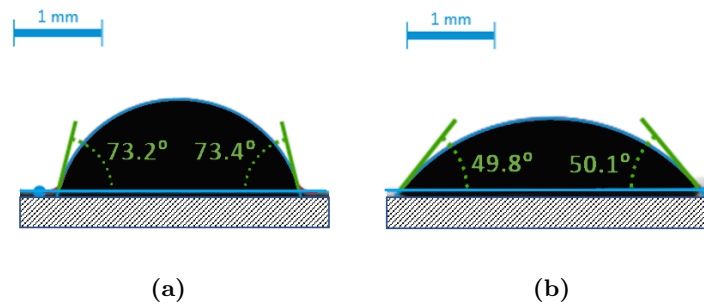
Figure 4: Snapsots for contact angle measurement for (a) bare tube and (b) Al_2O_3 + TiO_2 spray coated tube.
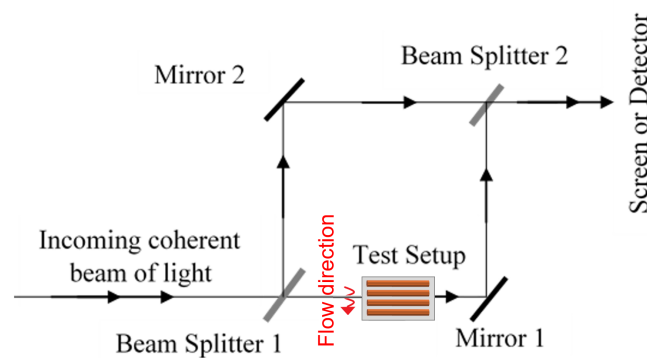
Figure 5: Ray diagram of MZI

reflected beam. The reflected beam and the transmitted beam superimpose at BS2 after being reflected by M1 and M2 respectively. The resulting interference pattern is captured using a frame grabbing device.

For the present study, the interferometer is operated in the infinite fringe mode where the two beams interfere to produce a fringe free field. Fringe development in this mode is only accompanied with a thermal disturbance at the test section. For the infinite fringe setting, a fringe is a line of constant phase, therefore, a line of constant refractive index so a constant density and hence, temperature (isotherm) (Muralidhar (2002),Krishnan Maliackal et al. (2017),Goldstein (1996)). For a two-dimensional temperature field, each fringe in an interferogram represents an isotherm, whereas for a three-dimensional field it is a constant line-averaged temperature. One fringe shift is generated by path length difference of λ, which is accounted for the temperature difference of ΔT_ϵ, which is given by the formula in Eq. 1.

$$\Delta T_\epsilon = \frac{\lambda}{(dn/dT)L_{eff}} \tag{1}$$

In order to evaluate the falling film interface temperature a set of fringe analysing procedures were formulated. A reference thermocouple is positioned at different stations near the vicinity of the falling film as shown in Fig. 6a. The essential distances needed for computing the interface temperature is represented in Fig. 6b

A non-linear temperature profile for varying radial position can be fitted for present scenario using Eq. 2.

$$T(r) = a + b(r - R - \delta_{mean}) + c(r - R - \delta_{mean})^2 \tag{2}$$

where r is the radial coordinate.

As one fringe shift is generated by path length difference of λ, Eq. 3 and Eq. 4 can be formulated.

$$
\begin{aligned}
\Delta T_\epsilon &= T_1 - T_2 \\
&= b\left[(r_1 - R - \delta_{mean}) - (r_2 - R - \delta_{mean})\right] \\
&\quad + c\left[(r_1 - R - \delta_{mean})^2 - (r_2 - R - \delta_{mean})^2\right]
\end{aligned}
\tag{3}
$$

$$
\begin{aligned}
\Delta T_\epsilon &= T_2 - T_3 \\
&= b\left[(r_2 - R - \delta_{mean}) - (r_3 - R - \delta_{mean})\right] \\
&\quad + c\left[(r_2 - R - \delta_{mean})^2 - (r_3 - R - \delta_{mean})^2\right]
\end{aligned}
\tag{4}
$$

Coefficients b and c can now be solved. The temperature gradient along radial direction is given by Eq. 5,

$$
\left(\frac{\partial T}{\partial(r - R - \delta_{mean})}\right)_r = b + 2c(r - R - \delta_{mean})
\tag{5}
$$

Now, T_2 can be calculated using an extrapolation step using the known reference temperature in same radial axis as shown by the Eq. 6.

$$
\begin{aligned}
T_2 &= T_{therm} + \frac{1}{2} \cdot \left[(r_{therm} - R - \delta_{mean}) - (r_2 - R - \delta_{mean})\right] \\
&\quad \cdot \left[b + 2c(r_{therm} - R - \delta_{mean}) + b + 2c(r_2 - R - \delta_{mean})\right]
\end{aligned}
\tag{6}
$$

Now coefficient a can be calculated, and hence the reference temperature can be reassessed with the known coefficients and the radial distance. If the error between the calculated and measured reference temperature is less than 8%, then T_3 is evaluated., T_3 can be found by using Eq. 7.

$$
T_3 = T_2 + T_\epsilon
\tag{7}
$$
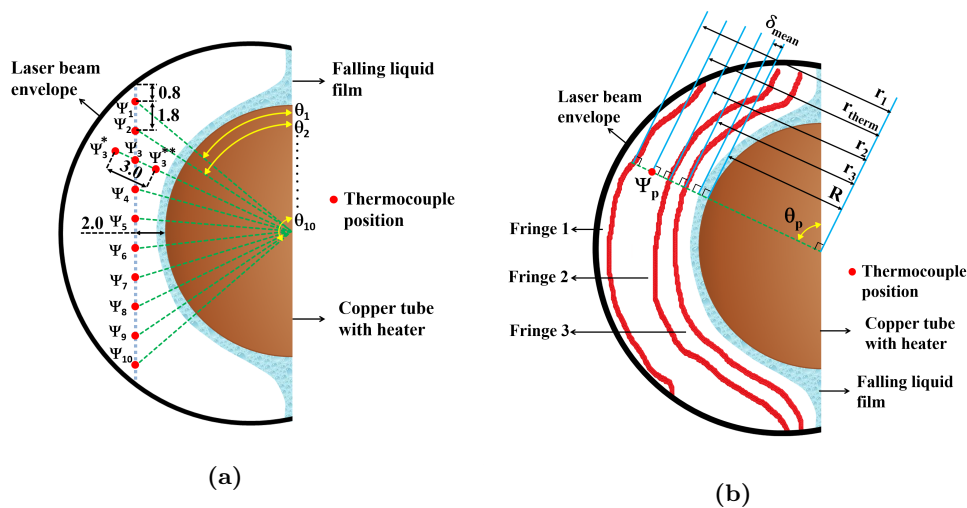
Figure 6: Schematic representation for quantitative analysis of interferogram (a) Various location for reference thermocouple (b) Distances involved for 'p'th position of thermocouple.

The falling film interface temperature can now be evaluated using Eq. 8

$$T_{interface} = a + b(r_3 - R - \delta_{mean}) + c(r_3 - R - \delta_{mean})^2 + T_3 \tag{8}$$

Interferograms were acquired using a CCD camera and zoom lens along with associated A/D converters. Sample interferograms for infinite fringe and heated cylinder with flow for steady state condition are shown in Fig. 7a and 8a respectively. ImageJ software package was used to analyse the fringes. A low band-pass filter and FFT image processing were carried out for every interferogram obtained. Intensity profiles for both interferograms are depicted in Fig. 7b and Fig. 8b. Each peak in the intensity profile corresponds to different isotherms in the interferogram. So once these radial positions are determined, the above mentioned interferometric method can be used to track the falling film interface temperature.

(a)

(b)
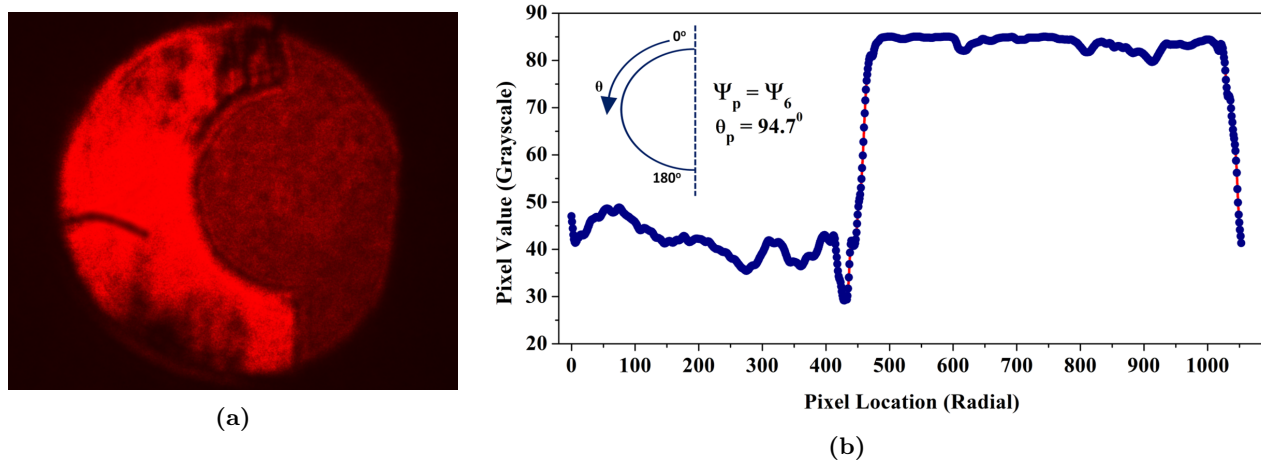
Figure 7: (a) Sample interferogram for infinite fringe mode and corresponding (b) Intensity profile for $\Psi_p = \Psi_6$ and $\theta_p = 94.7°C$

(a)

(b)
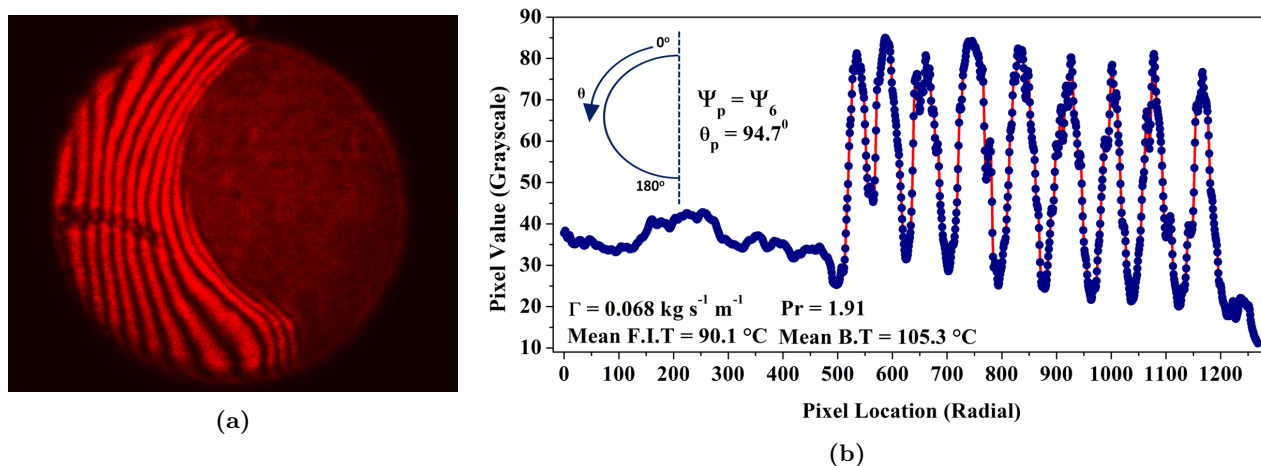
Figure 8: (a) Sample interferogram for steady state flow mode and corresponding (b) Intensity profile for $\Psi_p = \Psi_6$ and $\theta_p = 94.7°C$

In order to estimate T_ϵ, the effective length for each configuration has to be determined. Sobel filter, along with paint-brush algorithm was used to determine the edges of the flow. A direct measurement technique involving a digital camera and a pixel conversion factor was used to deduct L_{eff} from the processed image,

as shown in Fig. 9. For the present scenario, L_{eff} for the bare copper tube was found to be 163.8 mm and that for the $Al_2O_3 + TiO_2$ spray coated tube was 167.7 mm.

3.2 Falling film thickness measurement

A shadowgraphic method was implemented for measuring the local falling film thickness. The postulate that a laser beam propagating tangentially through a liquid medium on a cylinder wall will get blocked by the falling liquid film was used for deducting the film thickness data (Zhang et al. (2000)). The shadowgraphic images for bare tube without flow and with a steady flow are shown in Fig. 10a and Fig. 11a respectively. An inhouse Otsu's algorithm was developed in MATLAB to evaluate the local falling film thickness. A binarized image based on Otsu's threshold was generated for both the cases as shown in Fig. 10b and Fig. 11b. Otsu's threshold was interpreted by maximizing the inter class variance as depicted in Fig. 10c and Fig. 11c. The histograms (blue vertical bars) represent the pixel frequency for varying grayscale pixel intensity. The maxima of the interclass variance are represented by the blue dashed lines. A zoomed plot in the domain 0 - 80 is given in the inset to emphasize that the pixel frequencies are not zero in the mentioned region.

The radial intensity profile at $\theta = 50°$ was drawn for binarized image for the cases with and without flow as shown in Fig. 12. The pixel length corresponding to δ^* can be inferred by finding the abrupt change in the intensity (pixel value) as depicted in the plot. Now, the pixel length can be transferred to geometric length using Eq. 9. For this particular configuration, one-pixel length corresponds to 15.32μm geometric length.

$$\delta' = \delta^* \times GL \tag{9}$$

3.3 Error analysis

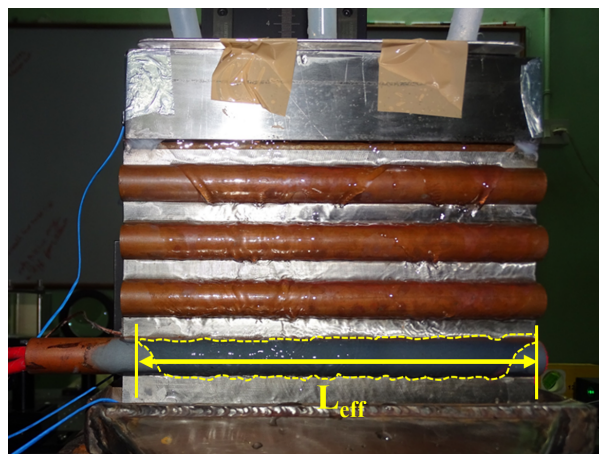The mean film thickness for each θ can be calculated by Eq. 10.

$$\delta_{mean} = \frac{\sum_{i=1}^{N} \delta_i'}{N} \tag{10}$$

The standard deviation for the entire population was as shown in Eq. 11.

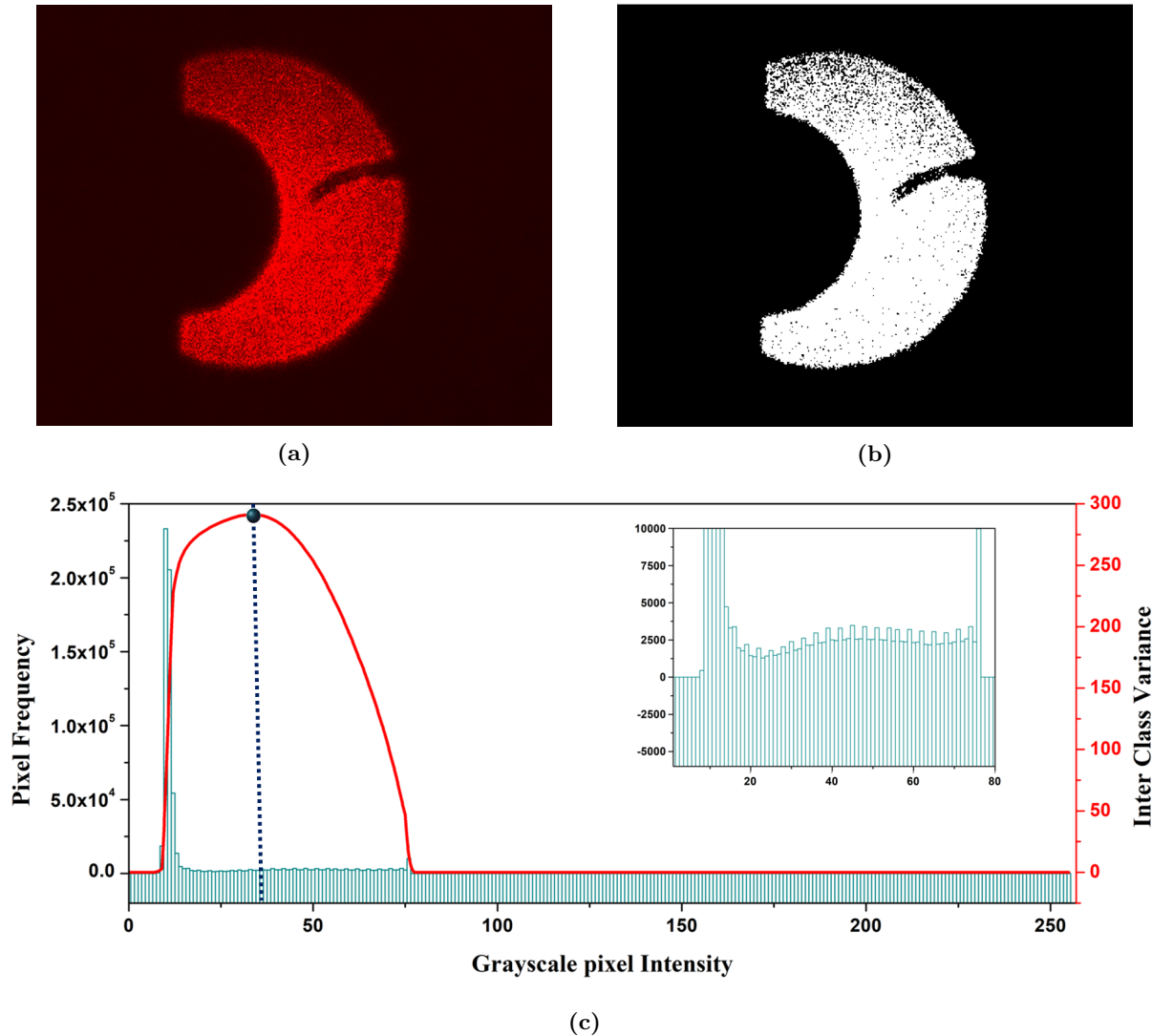$$SD = \sqrt{\frac{\sum_{i=1}^{N} (\delta_{mean} - \delta_i')^2}{N-1}} \tag{11}$$

The formula for finding SEM used was Eq. 12.

$$SEM = \delta_{mean} \pm \frac{SD}{\sqrt{N}} \tag{12}$$

Figure 9: Photograph of flow of falling film over $Al_2O_3 + TiO_2$ coated tubes.

(a)

(b)

(c)

Figure 10: (a) Real image and (b) Binary image of bare tube without flow. (c) Histogram of image along with inter class variance.

The sample population for plotting each data set was taken to be 30 images. The same error analysis was extended for falling film interface temperature measurement.

4. RESULTS AND DISCUSSION

4.1 Empirical relations
Equation 13 shows the empirical formula for the falling film thickness around the circumference of the cylinder given by Nusslet (Nusselt (1916)),

$$\delta = \left(\frac{3\mu_L \Gamma}{\rho_L \left(\rho_L - \rho_G \right) g \sin\theta} \right)^{1/3} \tag{13}$$

But, Eq. 13 was not taking account of the momentum effect of the falling film and thereby imparting errors to the calculation. Hou et al. (Hou et al. (2012)) proposed a modified formula for the same by appending

(a)

(b)

(c)
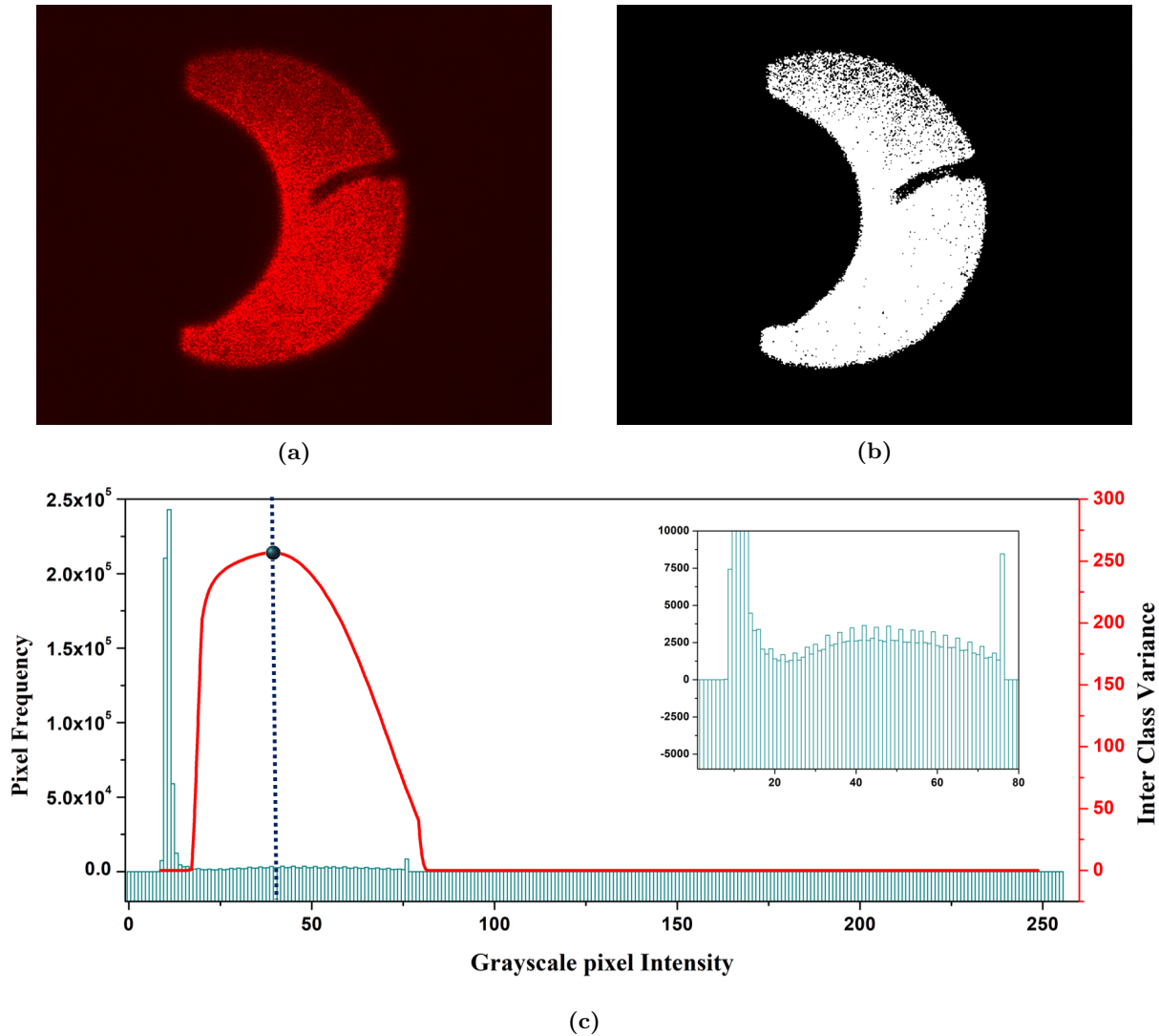
Figure 11: (a) Real image and (b) Binary image of bare tube with flow. (c) Histogram of image along with inter class variance.
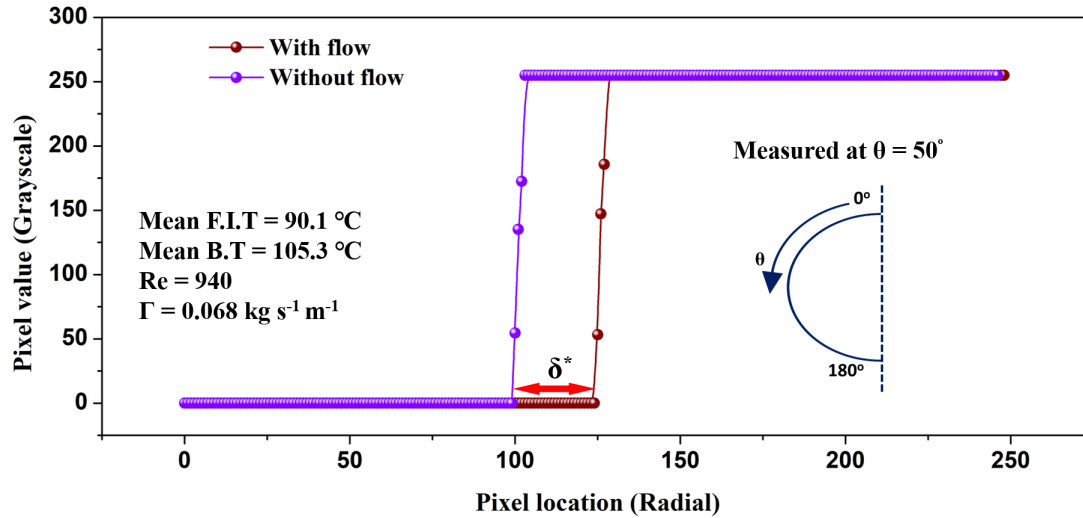
the terms to include the effect of impingement height as given by Eq. 14.

$$\delta = C\left(\frac{3\mu_L\Gamma}{\rho_L\left(\rho_L - \rho_G\right)g\sin\theta}\right)^{1/3}\left(\frac{S}{D}\right)^n \tag{14}$$

$$C = \begin{cases} 0.97540, 0° < \theta \leq 90° \\ 0.84978, 90° < \theta < 180° \end{cases} \qquad n = \begin{cases} -0.16670, 0° < \theta \leq 90° \\ -0.16479, 90° < \theta < 180° \end{cases}$$

where it is applicable in the range of $20 \leq D \leq 32$ mm, $10 \leq S \leq 40$ mm and $150 \leq Re \leq 800$, and Re for falling film flow around the wetted perimeter of the cylinder is given in Eq. 15,

$$Re = \frac{4\Gamma}{\mu_L} \tag{15}$$

Figure 12: Radial intensity profile at $\theta = 50°$ for the binarized image.

The present configuration investigates for values D = 15.9 mm, S = 9 mm and also for different surface roughness, which is outside the limit proposed by Hou et al. (Hou et al. (2012)).

4.2 Comparitive study of local falling film thickness

Figure 13 shows the comparative study of falling film thickness variation with varying circumferential angle for two different tube surfaces. Near to the entry region, local film thickness is showing an anomaly. It might be because for this particular configuration, before the film impinges the top surface of tube, it slides along a vertical wall to reach that point. It may have considerably reduced the momentum transfer resulting in increment of the local film thickness. For $\theta > 60°$, the local film thickness variation with empirical formula given by Hou et al.(Hou et al. (2012)) were found to be marginal. Comparing bare tube and $Al_2O_3 + TiO_2$ spray coated tube, the latter is exhibiting a lower film thickness because of higher porosity and increased wetting length for the same steady state boundary conditions.

### 4.3 Comparitive study of local falling film interface temperature

Figure 14 shows the local film interface temperature values for two different tubes for the same steady state boundary conditions. It can be seen from the plot that the thermal spray coated tube is exhibiting a higher interface temperature. The increase in interface temperature for the $Al_2O_3 + TiO_2$ coated tube can be attributed to lower local film thickness, turbulence, increased wettability and higher surface area.

5. CONCLUSIONS

In this paper, an optical shadow method (non-intrusive) was used to evaluate the falling film thickness around the circumference of a horizontal tube evaporator. A MZI was setup and utilized to visualize the isotherm formation and a novel interferometric method was developed to track the local falling film interface temperature. The studies were performed for two different tube surfaces, namely bare copper tube and $Al_2O_3 + TiO_2$ alloy coated tube.

The important conclusions that can be drawn from the present study are listed below:

- An Otsu's algorithm was developed to track the film thickness variation around the horizontal tube.

- $Al_2O_3 + TiO_2$ coated tube was exhibiting lower local film thickness values compared to bare coated tube. All the SEM values for the film thickness studies were found to be less than 11.3%.

- A novel interferometric falling film interface temperature tracking method was formulated and implemented.
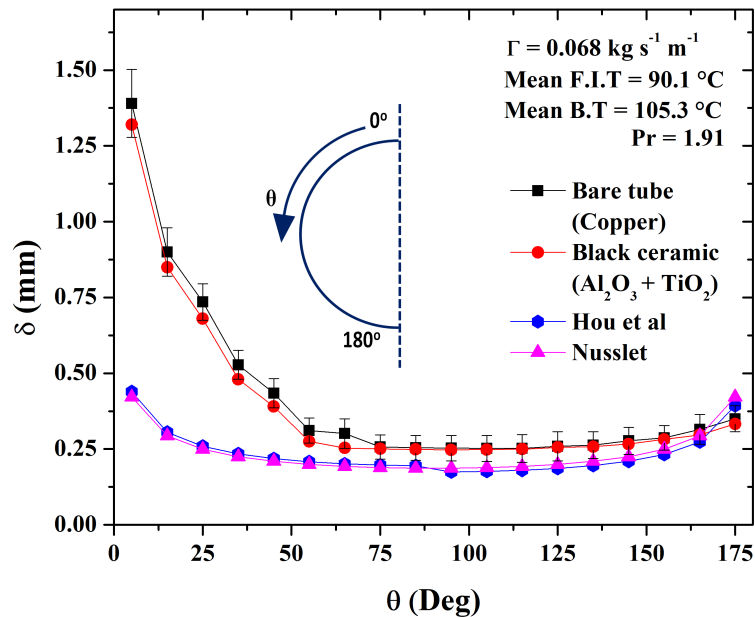
Figure 13: Variation of local falling film thickness with circumferential angle

- The thermal spray coated tube showed increased heat transfer characteristics compared to bare copper tube and a 63.6% increase in heat transfer rate was noted.

NOMENCLATURE

D	Tube diameter	(mm)
g	Acceleration due to gravity	$(m{\cdot}s^{-2})$
GL	Pixel conversion into geometrical length	(mm)
L	Length of the tube	(mm)
n	Refractive index	
N	Sample population	(mm)
Re	Falling film Reynolds number	
S	Impingement height	(mm)
SD	Standard deviation of the sample population	
T	Temperature	(˚C)

Subscript

eff	Effective quantity
G	Vapour state
i	Iteration
L	Liquid state
mean	Mean value
p	Cardinal value of reference thermocouple

Superscript

′	Quantity representing length scale
∗	Quantity representing pixel
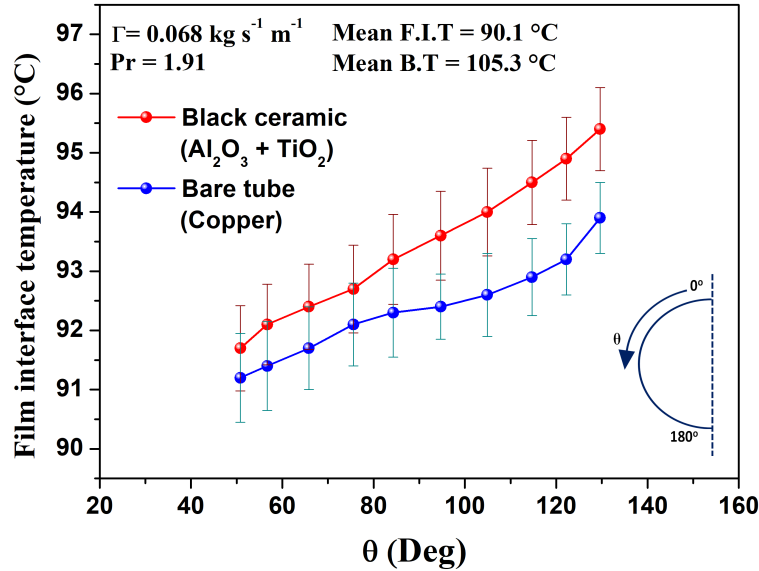
Figure 14: Variation of local falling film interface temperature with circumferential angle

Greek symbol

ϵ	Fringe shift	
θ	Circumferential angle	(degree)
ρ	Density	(kg·m^{-3})
μ	Dynamic visocity	$(\text{kg·m}^{-1}\text{·s}^{-1})$
Γ	Film flow rate per unit length on one side of the tube	$(\text{kg·m}^{-1}\text{·s}^{-1})$
λ	Wavelength	(nm)
δ	Falling film thickness	(mm)
Ψ	Position of the reference thermocouple	

Abbreviations

CCD	Charge Coupled Device
DAQ	Data Acquisition Unit
FFT	Fast Fourier Transform
F.I.T	Feed Inlet Temperature
F.O.T	Feed Outlet Temperature
LPM	Liters per minute
MED	Multi Effect Desalination
MZI	Mach Zehnder Interferometer
SEM	Standard Error of Mean

REFERENCES

Water Scarcity-UN Water factsheet on water security, United Nations. 2006. URL `Weblink:http://www.un.org/waterforlifedecade/scarcity.shtml`.

R. Abraham and A. Mani. Experimental studies on thermal spray-coated horizontal tubes for falling film evaporation in multi-effect desalination system. *Desalination and Water Treatment*, 56(1):71–82, 2015. ISSN 19443986. 10.1080/19443994.2014.937753. URL `http://dx.doi.org/10.1080/19443994.2014.937753`.

N. Borgetto, F. André, C. Galizzi, and D. Escudié. Simultaneous film thickness measurement and wall

temperature assessment by Low-Coherence Interferometry. *Experimental Thermal and Fluid Science*, 44:512–519, 2013. ISSN 08941777. 10.1016/j.expthermflusci.2012.08.013. URL `http://dx.doi.org/10.1016/j.expthermflusci.2012.08.013`.

X. Chen, S. Shen, Y. Wang, J. Chen, and J. Zhang. Measurement on falling film thickness distribution around horizontal tube with laser-induced fluorescence technology. *International Journal of Heat and Mass Transfer*, 2015. ISSN 00179310. 10.1016/j.ijheatmasstransfer.2015.05.016.

R. Goldstein. *Fluid Mechanics Measurements*. 1996. ISBN 156032306X.

D. Gstoehl, J. F. Roques, P. Crisinel, and J. R. Thome. Measurement of Falling Film Thickness Around a Horizontal Tube Using a Laser Measurement Technique Measurement of Falling Film Thickness Around a Horizontal Tube Using a Laser Measurement. 7632, 2010. 10.1080/01457630490519899.

H. Hou, Q. Bi, H. Ma, and G. Wu. Distribution characteristics of falling film thickness around a horizontal tube. *Desalination*, 2012. ISSN 00119164. 10.1016/j.desal.2011.10.020.

A. Jayakumar, A. Balachandran, A. Mani, and K. Balasubramaniam. Falling film thickness measurement using air-coupled ultrasonic transducer. *Experimental Thermal and Fluid Science*, 2019. ISSN 08941777. 10.1016/j.expthermflusci.2019.109906.

A. Krishnan Maliackal, A. Ganesan, and A. Mani. Experimental investigation of natural convection in a rectangular cavity with two protruded half cylinders using a Mach-Zehnder interferometer. In *Proceedings of SPIE - The International Society for Optical Engineering*, volume 10373, 2017. ISBN 9781510612037. 10.1117/12.2273716.

K.-Y. Law. Definitions for hydrophilicity, hydrophobicity, and superhydrophobicity: Getting the basics right. *The Journal of Physical Chemistry Letters*, 5(4):686–688, 2014. 10.1021/jz402762h. PMID: 26270837.

A. K. Maliackal, A. R. Ganesan, and A. Mani. Interferometric analysis of flow around a horizontal tube falling film evaporator for MED systems. *International Journal of Thermal Sciences*, 161(November 2020): 106745, 2021. ISSN 12900729. 10.1016/j.ijthermalsci.2020.106745. URL `https://doi.org/10.1016/j.ijthermalsci.2020.106745`.

K. Muralidhar. *Temperature field measurement in buoyancy-driven flows using interferometric tomography*, volume 12. jan 2002. 10.1615/AnnualRevHeatTransfer.v12.90.

W. Nusselt. Die oberflachenkondensation des wasserdamphes. *VDI-Zs*, 60:541, 1916. URL `http://ci.nii.ac.jp/naid/10014903553/en/`.

R. N. Wenzel. Surface roughness and contact angle. *The Journal of Physical and Colloid Chemistry*, 53(9): 1466–1467, 1949. 10.1021/j150474a015. URL `https://doi.org/10.1021/j150474a015`.

F. Zhang, J. Peng, J. Geng, Z. X. Wang, and Z. B. Zhang. Thermal imaging study on the surface wave of heated falling liquid films. *Experimental Thermal and Fluid Science*, 2009. ISSN 08941777. 10.1016/j.expthermflusci.2008.10.010.

J. T. Zhang, B. X. Wang, and X. F. Peng. Falling liquid film thickness measurement by an optical-electronic method. *Review of Scientific Instruments*, 71(4):1883–1886, 2000. ISSN 00346748. 10.1063/1.1150557.